Comparison of Wash-Coated Monoliths vs. Microfibrous Entrapped Catalyst Structures for Catalytic VOC Removal

Sabrina Wahid, Donald R. Cahela, and Bruce J. Tatarchuk
Dept. of Chemical Engineering, Center for Microfibrous Materials Manufacturing (CM3), Auburn University, Auburn, AL 36849

DOI 10.1002/aic.14555
Published online July 15, 2014 in Wiley Online Library (wileyonlinelibrary.com)

Head-to-head experimental performance comparisons for flow through pleated microfibrous structures (flat-, V-, and W-shaped) were made with wash-coated monolith of different cells per square inch (230 and 400). Microfibrous entrapped catalyst (MFEC) was prepared by entrapping support particles (γ-Al_2O_3, 150–250 μm diameter) into nickel microfibers. Pleated structures of MFECs and wash-coated monoliths containing Pd-Mn/γ-Al_2O_3 were investigated systematically for volatile organic compound (e.g., ethanol) removal at various face velocities (ca. 3–30 m/s) and at low temperatures ($\leq$473 K). The experimental studies showed that pleated MFEC (W-shaped) had shown significantly improved performance in VOC removal in terms of conversion and pressure drop than tested monolith for high face velocity system. The flexibility of pleating lowered the effective velocity inside the media that resulted lower pressure drop and higher conversion. Furthermore, a reaction kinetic model was developed for pleated MFEC considering the Peffer's model to substantiate the experimental results. © 2014 American Institute of Chemical Engineers *AIChE J*, 60: 3814–3823, 2014
Keywords: VOC removal, microfibrous entrapped catalyst, wash-coated monolith, heterogeneous contacting efficiency, reaction kinetics

Introduction

Background

The amount of research and development invested on new reactor design is comparatively scarce than that of catalyst synthesis, its improvisation by utilizing new materials and its characterization. Catalytic reaction applications which involve short contact time require a new formulation of heterogeneous contacting scheme. To achieve this goal, researchers are now paying more attention to the microstructured and/or microengineered systems which provide small characteristic dimensions and higher external surface area.[1–4] Microfibrous entrapped catalyst (MFEC) and sorbent (MFES) exhibited significant benefits in heterogeneous catalysis and adsorption applications.[5–7] MFEC offers a new approach for creating a small, efficient, and lightweight heterogeneous contacting system. Microfibrous entrapped ZnO/SiO_2 has proved remarkable improvement over packed beds[8–11] in hydrogen reformate streams of gas-phase desulfurization. Microfibrous entrapped small particulates has produced high contacting efficiency sorbents suitable for applications demanding high levels of contaminant removal. Advantages of MFES over packed bed of small adsorbent particles has been experimentally demonstrated and investigated in terms of axial dispersion effects.[12] Furthermore, for single pass removal of molecular contaminants, that is, ozone[13] and VOCs[14] (e.g., ethanol, toluene, and *n*-hexane), pleated MFEC has shown promising performance which promoted the authors to investigate the experimental performance comparison among the conventional reactor systems. Pleated MFEC can lead to higher reactions rates and lower pressure drops due to smaller characteristic dimensions and reduced effective velocity compared to the other heterogeneous contacting systems.

The authors have mentioned the importance and the mechanistic details of VOC removal for high performance platforms, for example, military ships, tanks, aircraft cabin air, and so forth in their previous study.[14] Among the toxic air pollutants regulated by EPA, 90% belongs to VOCs. The authors had considered the aforementioned VOCs based on the survey conducted by Nagda and Rector.[15] In this study, ethanol was considered among the aforementioned VOCs. Catalytic ethanol removal at high mass flow rates was performed experimentally using different dimensional structured reactors (Pd-Mn/Al_2O_3 as catalyst), for example, wash-coated monoliths of various cells per square inch (CPSI), and MFEC with various pleat numbers, based on the theoretical investigation conducted by Kalluri et al.[13] for ozone removal. The theoretical investigation showed that while packed bed had resulted higher pressure drops and monolith had caused low fluid-solid mass-transfer rates, pleated MFEC had shown significantly improved performance in ozone removal. However, this theoretical investigation required an experimental verification. Therefore, a performance evaluation parameter, heterogeneous contacting efficiency (η_{HCE}), was applied to evaluate the performance of those aforementioned reactor geometries.[14] Balakotaiah and West[16] and Giani et al.[17] have also considered this parameter

Correspondence concerning this article should be addressed to B. J. Tatarchuk at tatarbj@auburn.edu.

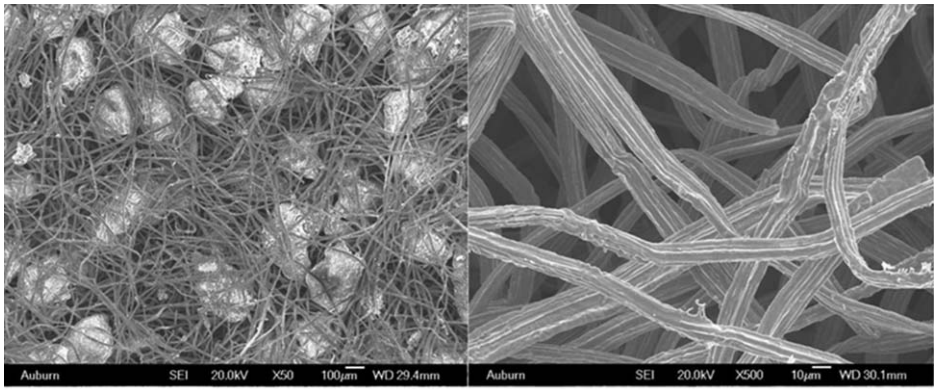

Figure 1. Micrograph of (a) 150–250 μm Al_2O_3 entrapped in 8 m sintered Ni fiber; (b) cylindrical Ni fiber with the ridges on the surface.

for comparing the performance of monolith with packed bed and catalytic foam. Many performance features, for example, pressure drop, chemical conversion, amount of catalyst utilization, cost of construction, catalyst life, and so forth would be involved in evaluating the overall performance of a reactor system. As it is difficult to define one single parameter which will consider all these aforementioned features, chemical conversion and pressure drop across the reactor were considered in this study. This parameter relies on the logarithmic removal of reactant concentrations per unit of pressure drop. This is a dimensionless number, defined as the product of mass efficiency (i.e., conversion achieved) to flow efficiency (i.e., inverse of pressure drop), per unit surface area of the catalyst (a measure of catalyst utilization). However, the experimental comparisons were restricted only to monolith and MFEC considering the practical difficulties of construction and testing of packed beds with the existing apparatus and operating conditions of the experiments.

The underlying mechanism behind the enhanced reactivity of microfibrous media requires investigation. To understand the basic physical and chemical characteristics of MFEC and optimizing the effectiveness and performances, a reaction kinetic model was established for pleated MFEC using Peffer's equation[18] in order to investigate the reaction kinetics. The reaction kinetic model will provide a deep insight on the global reaction kinetics occurred in the pleated structure of MFEC at high face velocities.

Microfibrous entrapped catalyst

MFECs developed by Auburn University, are designed for chemical and electrochemical applications. Figures 1a, b show SEM images of MFEC consisting of 150–250 μm Al_2O_3 entrapped in 8-μm Ni microfibers and the cylindrical-shaped Ni microfibers (8 μm) with ridges on the surface, respectively. These microengineered heterogeneous contacting materials are composite structure of fibers (2–20 μm) that can entrap small catalyst particulates (50–300 μm). The catalyst particles are held in space by three-dimensional (3-D) sinter-locked networks of microfibers, resembling a "frozen-fluidized bed." The choice of fiber materials can be metals (e.g., copper, nickel, and stainless steel), glass or polymer, conditional to the process consideration. The properties of the fiber can be tailored which rely on the process requirement. The surface area of MFEC can vary roughly from 1.5 to 1500 m^2/g, depending on the fraction of higher surface area material. The distinctive volume loading of catalyst and fibers in MFEC are about 10–25 and 1–5%, respectively, with rest being void. However, voidage of these materials can be adjusted from 98% down to values similar to a packed bed.

MFEC possesses many inherent beneficial properties. Due to the exclusive ability to entrap small catalyst particles, MFECs exhibit a great promise to increase intraparticle and interparticle mass-transfer rates, as opposed to the larger particles typically used in the conventional packed bed systems. MFECs are prepared by the wet lay process, in which the microfibers and the particles settle in a highly viscous medium (water); this assemblage of particles is self-correcting and hence leads to a uniform structure. This structural uniformity eliminates "channeling" or "flow maldistribution." The high voidage and the high aspect ratio (length to diameter) of fibers in MFECs decrease the axial dispersion, improve the radial dispersion, and create a plug flow like condition. Furthermore, high voidage in MFECs helps to reduce the pressure drop significantly. Moreover, another unique feature of MFECs is the flexibility of pleating, which helps to achieve higher conversion and to lower the pressure drop.

Reaction Kinetic Modeling for Pleated MFEC

Ethanol removal is a highly exothermic reaction, however, due to the low concentration involved in this research; no significant temperature rise was observed in the reactor. Furthermore, the reactor *Pe* numbers were considerably high ($Pe \approx 32$–83) due to the high face velocity involved in this process. This indicates to the isothermal plug flow condition.[19] The gas-phase differential equation for reactant A in any plug flow reactor is given by Eq. 1

$$-\frac{v_o}{\mathrm{PF}}\frac{dC_A}{dx} = k_m x_c (1-\varepsilon_b)(C_A - C_S) \tag{1}$$

To predict the gas–solid mass-transfer coefficient in MFECs, the Peffers's model (Eq. 2) was applied,[20] which is applicable for low *Re* number and high *Pe* number. Peffer's equation was specifically proposed for particulate beds operating in laminar flow conditions. The pleated formation and small characteristic dimension of the MFECs enhances the laminar behavior inside the media even though the inlet velocity is high. In this study, the flow inside the pleated MFEC was laminar with very little lateral mixing caused by the fibers. Another reason for applying this equation was

because it considers the bed voidage. Most of the other semi-empirical correlations widely used for estimating mass-transfer coefficients of packed beds are applicable for a limited voidage range. PF term (Eq. 3) was also included in this equation due to the decreased velocity inside the pleated MFEC. The effect of fibers on mass-transfer rates was studied using computational fluid dynamics simulations and was found to be insignificant for low Re.[20] Hence, the presence of the fibers was neglected in mass-transfer calculation for MFEC. However, it was considered for bed voidage calculations

$$Sh = 1.26\left(\frac{1-\gamma^5}{W}\right)^{\frac{1}{3}}\left(\frac{Re_p}{PF}Sc\right)^{\frac{1}{3}} \quad (2)$$

$$PF = \frac{\text{Total face area of MFEC media}}{\text{Total cross-sectional area of the reactor}} \quad (3)$$

The mass-transfer rate to the catalyst surface in the above expression (Eq. 1) should be equal to the surface reaction rate inside the catalyst. The assumption is that the catalytic VOC removal follows first-order reaction kinetics[21,22]

$$k_m(C_A - C_S) = \eta k_r C_S \quad (4)$$

The intraparticle transport rates were estimated using the following effectiveness factor correlation (Eq. 5), which involves Thiele modulus. The relation between the effectiveness factor and the Thiele modulus indicates the diffusion and reaction limitation phenomena[19]

$$\eta = \frac{1}{\Phi}\left(\coth(3\Phi) - \frac{1}{3\Phi}\right) \quad (5)$$

$$\Phi = \left(\frac{\varphi_p d_p}{6}\right)\sqrt{\frac{k_r}{D_e}} \quad (6)$$

For the pleated geometries compared in this study, the effective diffusivity of ethanol inside the catalyst support followed Eq. 7 with the values of $\tau_p = 3.0$ and $\varepsilon_p = 0.82$. These values of intraparticle tortuosity and porosity resemble to the γ-Al_2O_3 particles used in the experiments

$$D_e = D_m\frac{\varepsilon_p}{\tau_p} \quad (7)$$

The molecular diffusivity (D_m) of ethanol in the air was estimated using Fuller's method, as shown in Eq. 8.[23] All the other gas properties considered in this study are based on the operating conditions

$$D_m = \frac{0.00143T^{1.75}}{PM_{AB}^{\frac{1}{2}}\left[\left(\sum_v\right)_A^{\frac{1}{3}} + \left(\sum_v\right)_B^{\frac{1}{3}}\right]^2} \quad (8)$$

k_{eff} is the effective reaction rate per unit volume of catalyst, which is defined by Eq. 9. This is a function of both mass-transfer coefficient and reaction rate constant. The balance among Eqs. 1, 4, and 9 results Eq. 10. Integration of Eq. 10 results in Eq. 11

$$\frac{1}{k_{eff}} = \frac{1}{k_m} + \frac{1}{\eta k_r} \quad (9)$$

$$-\frac{v_o}{PF}\frac{dC_A}{dx} = k_{eff}x_c(1-\varepsilon_b)C_A \quad (10)$$

$$\text{Conversion} = 1 - \exp\left[-k_{eff}x_c(1-\varepsilon_b)\frac{L}{v_o/PF}\right] \quad (11)$$

Experimental Details

MFEC preparation

MFEC was prepared by the wet lay paper making technique. Nickel fibers (12.5 g) (Ni-200, 8-μm nominal diameter) and 1.5 g of cellulose were dispersed in high viscosity water. The viscosity of the water was modified by the addition of 0.8% (w/w) hydroxy ethyl cellulose (HEC) followed by hydrolysis of HEC at pH ~10 using sodium hydroxide. After the addition of Ni fibers and cellulose to the modified water, the mixture was stirred in a blunt propeller to disperse the Ni fibers. To ensure proper dispersion of the Ni fibers, initially the stirring was conducted at low RPM. At this stage, most of the Ni fibers were dispersed, and the mixture was then stirred at high RPM to disperse the few Ni fibers still in bundles. The viscosity modifier of water and the two-stage mixing helped to disperse the fibers without excessive reduction in their aspect ratio. Then, the suspension of fibers and cellulose were placed on a 20.32 × 20.32 cm^2 hand sheet former. The suspension was stirred vigorously and 25 g of aluminum oxide particles (150–250 μm) were added to the suspension in the sheet former. The excess water inside the sheet was drained, and thereby, the preform of MFEC, a 3-D structure consisting of fibers, cellulose, and particles, was formed. Protective layers, containing only Ni fibers and cellulose, were also prepared in the similar fashion. Main media was composed of two protective layers and one particles incorporated layer, as a "sandwich" format. Cellulose acts as a binder for the Ni fibers that provide wet and dry strength to the preform due to the hydrogen bonding between cellulose fibers. The preform was dried at 373 K for 2 h. Afterward, this perform was oxidized at 723 K to remove the cellulose. Subsequently, the media was sintered at 1173 K for 40 min using hydrogen. In this stage, fibers were bonded to each other and prepared a sinter-locked structure. Thus, MFEC was prepared. The samples were placed between two 25.4 × 25.4 × 0.15 cm^3 tight thickness tolerance steel plates with washers, used as spacers between the plates, to define the final thickness of the nickel MFECs.

Catalyst preparation and characterization

$Pd(NO_3)_2$ solution and $Mn(NO_3)_2$ solution ($Pd(NO_3)_2 \cdot 2H_2O$ and $Mn(NO_3)_2 \cdot 4H_2O$ from Alfa Aesar) were used to wet impregnate the γ-Al_2O_3 particles in microfibrous media. For preparing the Pd-Mn catalyst, 0.1 M $Pd(NO_3)_2$ solution and 1.98 M $Mn(NO_3)_2$ solution were mixed. Pd is used widely in VOC abatement due to its stability and higher activity. Finally, the impregnated MFEC samples were dried at 373 K and calcined at 748 K for 4 h. Thus, MFEC sheets with PdO-MnO_x/γ-Al_2O_3 were prepared. The amounts of Pd and Mn in the catalysts were determined by inductively coupled plasma-atomic emission spectroscopy (Hazen Research), which is shown in Table 1. The amount of individual metal catalyst load for MFECs and wash-coated monoliths was constant.

For experimental comparison, ceramic honeycombs (Synthetic cordierite, $2MgO \cdot 2Al_2O_3 \cdot 5SiO_2$) from Applied Ceramics of 230 and 400 CPSI were used for the catalyst preparation. The support particles were loaded onto the ceramic substrate by sol-gel technique.[24–27] In this case 1:2:5 (wt) of urea, 0.3 M HNO_3, and boehmite (CATAPAL B of packing density 800–1100 kg/m^3, from Sasol) were used. The substrate was immersed into the solution for 5 min followed by the removal of the excess solution by flowing air

Table 1. Metal Content of the Tested Catalyst

Metal Content (wt %)	MFEC	Monolith
Pd	3.59	1.83
Mn	7.57	4.84

through the substrate. The substrate was dried at 393 K and subsequently calcined at 773 K for 6 h. These steps were continued until 30 g support was loaded onto the substrate which possessed equal amount pore volume as the MFEC possessed. The wash-coated monolith was then impregnated by $Pd(NO_3)_2$ and $Mn(NO_3)_2$ solution. These were subsequently dried and calcined at the same temperature as conducted for MFEC. These loaded monoliths had equal amount of metal which matches MFEC contained. Hence, each monolith and MFEC had equal amount of pore volume and metal content. However, the particle size of γ-Al_2O_3 in wash-coated monoliths and MFECs were significantly different due to the differences in their structure and preparation technique. Figure 2 shows the SEM images of monolith before and after applying the wash-coat.

Test setup

The bed properties and the pleat numbers of MFEC, and the structural properties of monoliths, used in this study are listed in Tables 2 and 3, respectively. Figure 3 shows the uniquely designed system for testing microfibrous material to achieve catalytic VOC removal at microsecond contact time.[14] The test setup consists of a high pressure 40 hp radial blower (Fan Equipment Company), which circulates air inside the closed-loop system. A variable speed drive is used to control the system speed, which can reach over 30 m/s inlet velocity. Heaters as well as purging air are used to control the system temperature, which can be raised to as high as 473 K. The main reactor section is square shaped and has a dimension of $12.7 \times 12.7 \times 22.9$ cm^3. The MFEC formations were flat, V-shaped, W-shaped which correspond to the numbers of pleat 1, 2, and 4, respectively, (Figure 4). The dimension of the monolith was $12.7 \times 12.7 \times 11.45$ cm^3. Therefore, two monoliths were placed in series to make the length equal to MFEC structure. As shown in Figure 5, the prepared MFECs were placed in aluminum U-shaped channels to form the structure. Compressed air was used to vaporize ethanol and mixed with the air stream from the blower to obtain the desired challenge gas concentration (100 ppmv) at the inlet of the reactor. The operating conditions are listed in Table 4.

Results and Discussions

Experimental comparison

Figure 6 shows experimentally obtained pressure drops at different velocities for various reactor formations. The construction and operation of the packed beds may not be feasible in practice for the operating conditions (velocity used

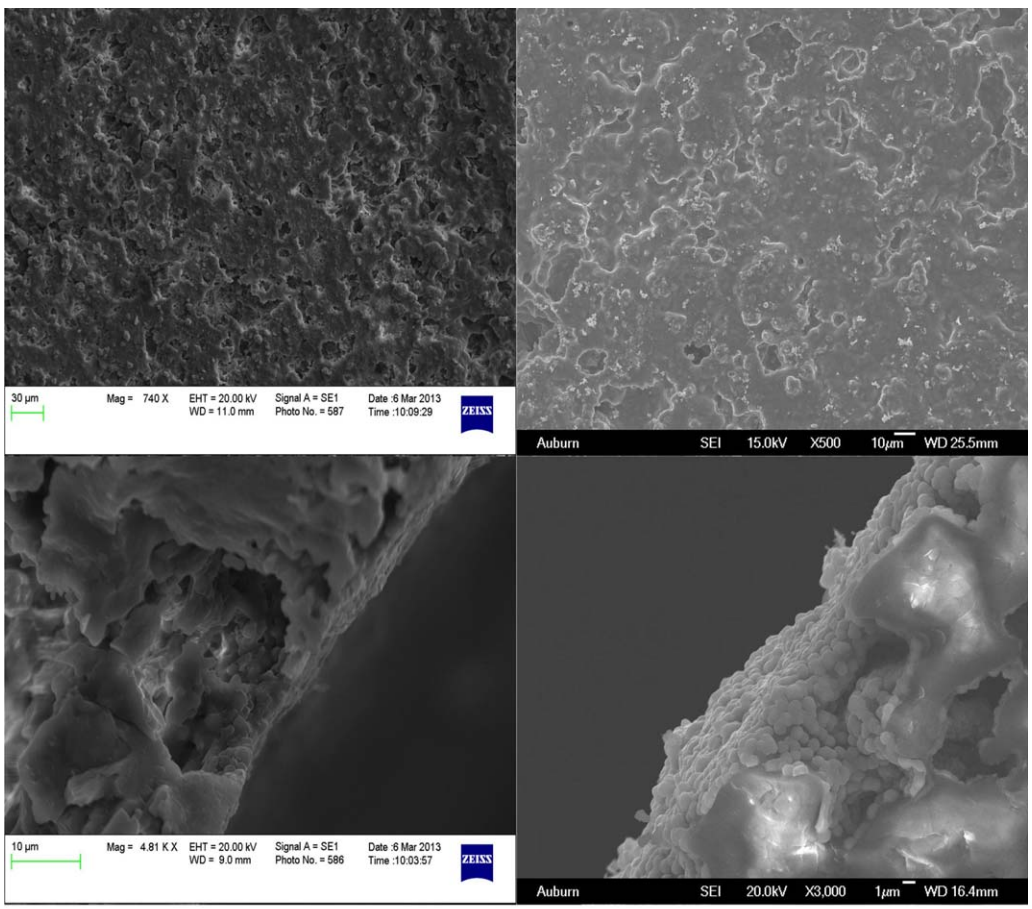

Figure 2. Micrograph of monolith (change in the structure after wash-coating the surface).

[Color figure can be viewed in the online issue, which is available at wileyonlinelibrary.com.]

Table 2. Properties of the MFEC

Numbers of pleat	1, 2, and 4
Thickness (mm)	3.6
Nominal fiber diameter, d_f (μm)	4, 8, and 12
Particle diameter, d_p (mm)	0.19
Catalyst particle sphericity, φ_p	0.7
Fiber sphericity	1.05 (= 1.5 × 0.7)
Catalyst (vol %)	11.1
Metal (vol %)	2.2
Void (vol %)	86.7

and mobile settings) used in this application, as this would require construction of extremely thin ($\leq$ MFEC thickness) packed beds for keeping the pressure drop sufficiently low. Therefore, packed beds were not included in this study. The plot exhibits that W-shaped MFEC had relatively low pressure drop than the other tested structures. This can be attributed to the fact that an increase in pleat number reduced the effective velocity inside the media, which thereby, reduced the pressure drop. However, flat-shaped and V-shaped MFECs showed relatively higher pressure drop than wash-coated monoliths despite of the media having higher voidage. This is because monoliths offered low resistance to flow due to straight channel. Hence, experimental pressure drop occurring across different reactor geometries showed the following order: flat-shaped MFEC > V-shaped MFEC > 400 CPSI monolith > 230 CPSI monolith > W-shaped MFEC.

The experimental ethanol conversion comparison among MFECs of flat-shaped and W-shaped design, monoliths of 230 CPSI, and of 400 CPSI are shown in Figure 7. In all cases, the total amount of metal loading and the operating conditions were kept constant. For both flat-shaped and W-shaped MFECs, the thickness of the media was same. Conversions of all cases decreased with the increase of inlet velocities. These high gas velocities indicated low intralayer residence times inside the catalytic structure which had resulted short contacting reaction. The low conversion for all cases can be attributed to the fact that overall reaction rates were limited by surface reaction rate as the compound diffuses through the pore mouth of the catalyst rapidly. Furthermore, the system temperature (<473 K) was not high enough for the ethanol to undergo complete removal due to the limitations in the design of the present test apparatus. However, the experimental temperatures in this study were chosen so as to match the operational range of the high performance platforms (e.g., commercial aircraft cabin). Though, a change in operating conditions would not alter the reactivity order of different geometries which is as follows: W-shaped MFEC > 400 CPSI monolith > 230 CPSI monolith > flat-shaped MFEC. The reason behind monoliths and flat structures having comparatively low conversion than W-shaped MFEC can be attributed to the relatively low gas–solid mass-transfer rates and higher intralayer residence time inside the media due to the pleated geometry. Pleated

Table 3. Properties of the Monolith

Cells per square inch (CPSI)	230	400
Wall thickness, t_w (0.001 in./μm)	8/203	6.5/165
Catalyst washcoat thickness, t_c (μm)	12.5	12.5
Channel diameter, d_{ch} (mm)	1.422	1.054
Void (vol %)	72.13	68.89
Catalyst (vol %)	3.484	4.685

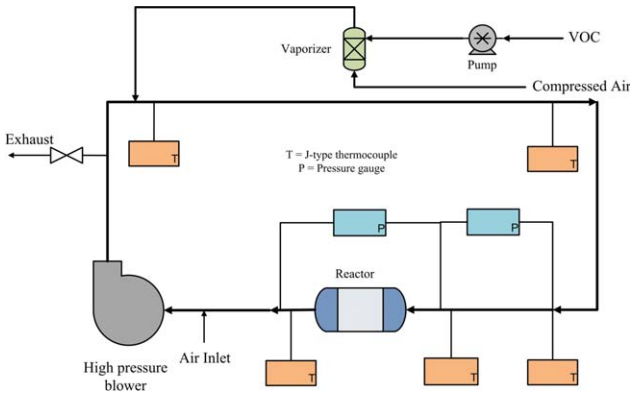

Figure 3. Schematic diagram of the experimental setup.

[Color figure can be viewed in the online issue, which is available at wileyonlinelibrary.com.]

geometry reduces the effective velocity inside media by the factor of PF term, which thereby increases the intralayer residence time. Furthermore, the properties (e.g., pore volume and particle density) of the support particle of wash-coated monolith and MFECs were not the same.

Based on the experimental pressure drop and ethanol conversion data, the η_{HCE} values were calculated using Eq. 12 and shown in Figure 8. As for both pressure drop and conversion measurements, W-shaped MFEC exhibited improved performance than the other tested geometries, the η_{HCE} values for this structure were considerably higher for the same operating conditions. In this study, pleat number was

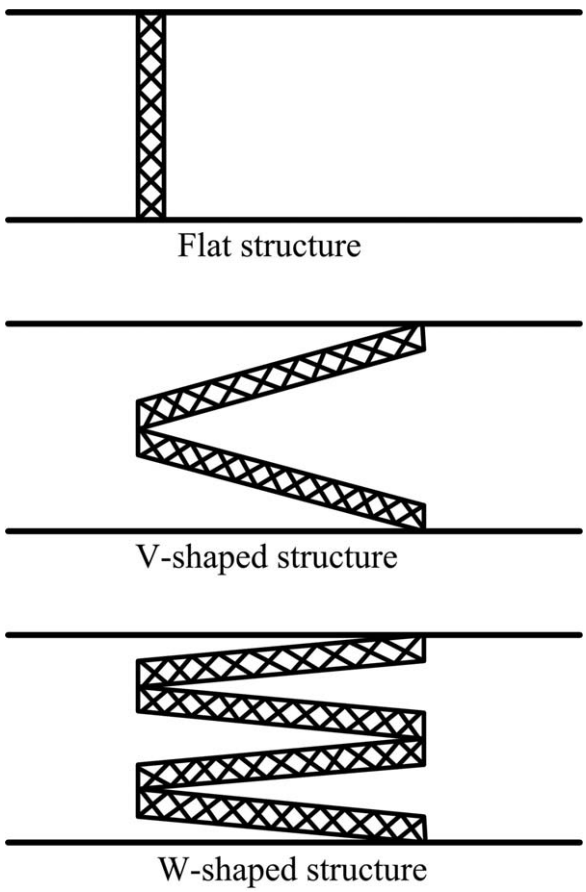

Figure 4. Schematic diagram of various MFEC reactors.

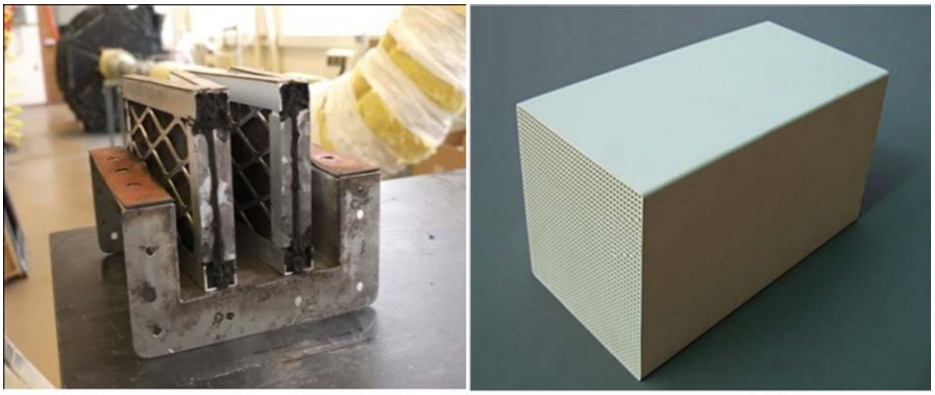

MFEC Monolith

Figure 5. Structures those were experimentally tested.

[Color figure can be viewed in the online issue, which is available at wileyonlinelibrary.com.]

restricted to 4, although this value can be raised further. However, a further raise in pleat number might negatively affect the advantages of pleating. Furthermore, wash-coated monoliths were restricted to 230 CPSI and 400 CPSI due to manufacturer limitation

$$\eta_{HCE} = \frac{1}{2}\rho v_o^2 \frac{\log\left(\frac{C_{Ai}}{C_{Ao}}\right)}{-\Delta P} \tag{12}$$

To verify this experimental performance comparison, theoretical η_{HCE} values of the tested geometries were calculated for ethanol conversion. To achieve the theoretical η_{HCE} value, it is essential to consider mass-transfer and momentum transfer correlation for both monoliths and pleated MFECs. For monoliths, well established mass-transfer correlation[28] and friction factor correlation[29] were used. Table 5 shows the friction factor correlation and mass-transfer correlation those are considered in this study. For a first-order reactor kinetics, maximum conversion is attainable when the

Table 4. Operating Conditions

Temperature (K)	423–473
Pressure (kPa)	101.3
Inlet velocity (m/s)	3–30
Challenge gas	Ethanol
Inlet concentration (ppmv)	100

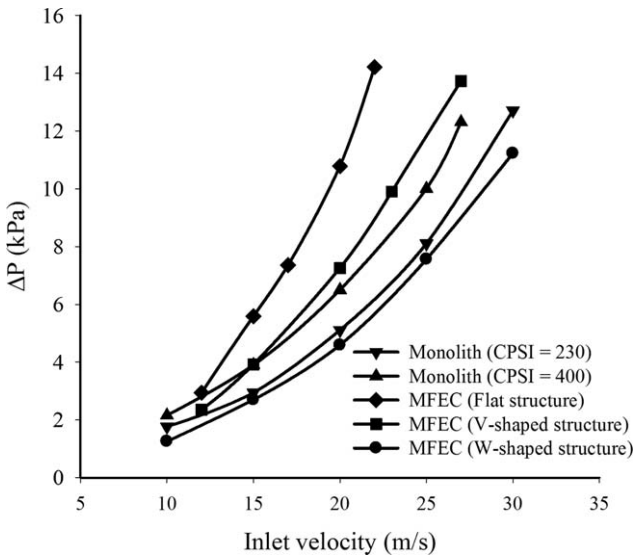

Figure 6. Experimental pressure drop occurring across different catalytic structures for various inlet velocities ($T = 473$ K).

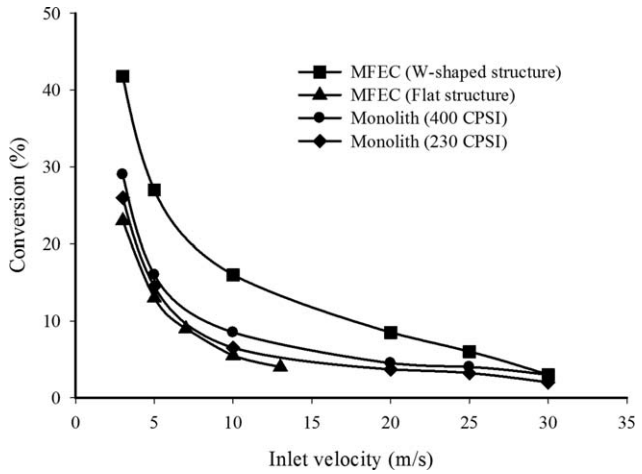

Figure 7. Ethanol conversion vs. inlet velocity using different catalyst structures ($T = 473$ K).

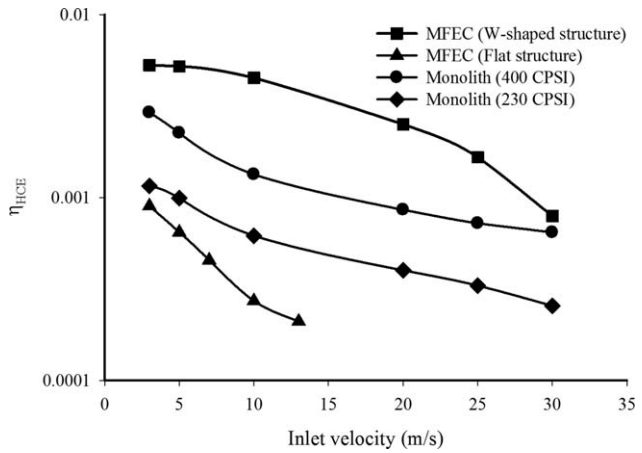

Figure 8. Experimentally obtained heterogeneous contacting efficiency for different catalytic structures at different inlet velocities ($T = 473$ K).

Table 5. Friction Factor and Mass-Transfer Correlations Used in this Study for Pleated MFEC and Wash-Coated Monolith

Correlation	Pleated MFEC	Wash-coated monolith
Friction factor (f)	$f=\mathrm{Cr}\times\left\{72\left[\left(\sum\frac{x_i\varphi_p d_p}{\varphi_i d_i}\right)^2+x_{FD}\sum x_i\left(\frac{\varphi_p d_p}{\varphi_i d_i}\right)^2\right]\frac{(1-\varepsilon_b)}{PFRe_p}+3\frac{\tau_b}{\cos\theta}\frac{1}{PF^2}\right.$ $\left.\left[C_f+C_{FD}\frac{\varepsilon_b}{4}\right]\sum\left(\frac{x_i\varphi_p d_p}{\varphi_i d_i}\right)\right\}\frac{(1-\varepsilon_b)}{\varepsilon_b^3}\frac{\tau_b^2}{\cos^2\theta}$ $\mathrm{Cr}=\left(1.651x_c^2-1.357x_c+1\right)\left[1-0.1x_c\left(\frac{\varphi_p d_p}{(\varphi_p d_p)_{\text{average particle size}}}-1\right)\right]$	$f_F=\frac{13}{\varepsilon_b Re_{ch}}$ for $\frac{Re_{ch}}{\varepsilon_b}<1000=\frac{0.03}{\varepsilon_b^{1.88}Re_{ch}^{0.12}}$ for $\frac{Re_{ch}}{\varepsilon_b}>1000$
Mass Transfer (Sh)	$Sh=1.26\left(\frac{1-\gamma^5}{W}\right)^{\frac{1}{3}}\left(\frac{Re_p}{PF}Sc\right)^{\frac{1}{3}}$	$Sh=2.967+8.827\left(\frac{1000}{Gz}\right)^{-0.545}\exp\left(\frac{-48.2}{Gz}\right)$

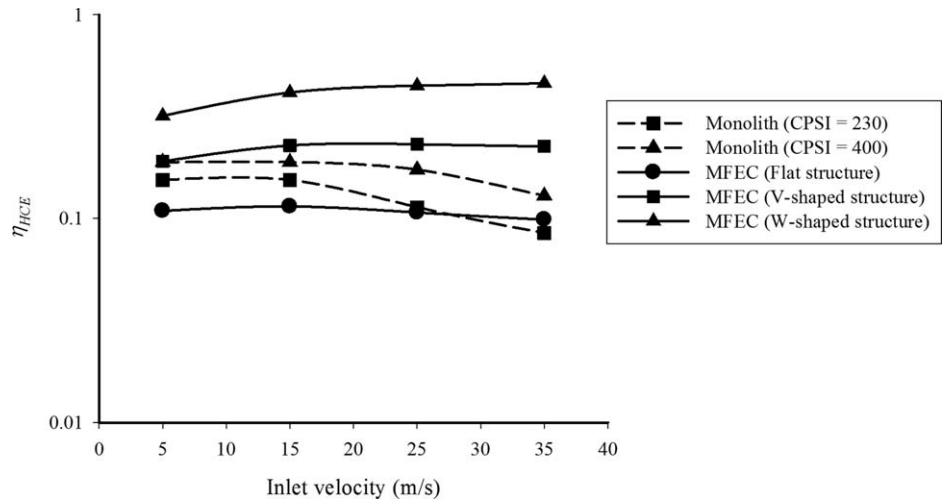

Figure 9. Theoretical heterogeneous contacting efficiency vs. inlet velocity for different catalytic structures (T = 473 K).

reactor is operated in a complete gas–solid mass-transfer controlled regime[30], that is, $C_{As}=0$. Integration of Eq. 1 results in Eq. 13

$$\log\left(\frac{C_{Ai}}{C_{Ao}}\right)=k_m x_c(1-\varepsilon_b)\left(\frac{L}{v_o/\mathrm{PF}}\right) \tag{13}$$

The pressure gradient occurring across monoliths and MFECs can be described by a general equation, as shown in Eq. 14, where f is the friction factor and d_c is the characteristic length, specific for each reactor type. The characteristic length (d_c) of MFECs is equal to the effective particle diameter ($\varphi_p d_p$) whereas for monoliths, it is equal to the channel diameter (d_{ch})

$$-\frac{\Delta P}{L}=\frac{1}{2}f\frac{\rho v_o^2}{d_c} \tag{14}$$

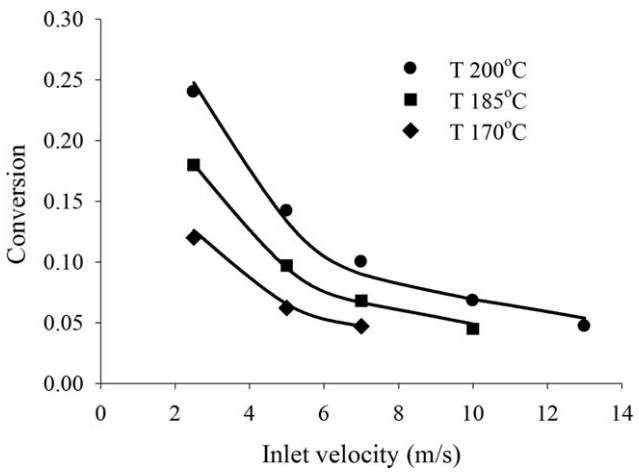

Figure 10. Comparison between model prediction and experimentally obtained conversion at different inlet velocities using flat structure of MFEC.

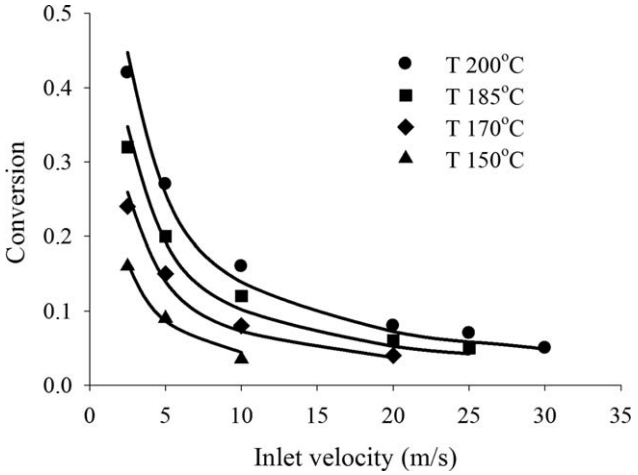

Figure 11. Comparison between model prediction and experimentally obtained conversion for different inlet velocities using W-shaped structure of MFEC.

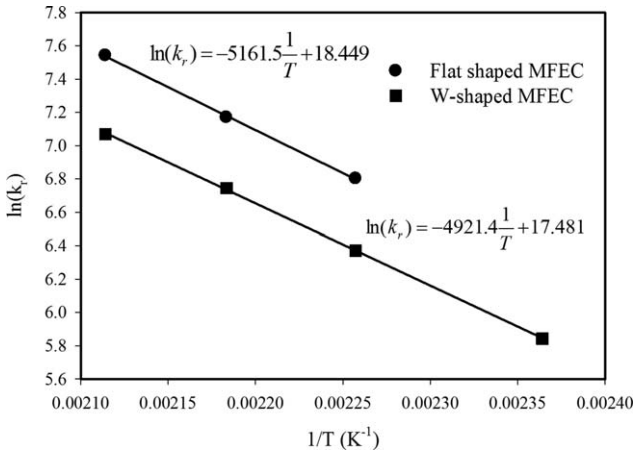

Figure 12. Arrhenius plot for catalytic VOC removal reaction for different pleated MFEC.

Substitution of Eq. 14 for pressure drop and Eq. 13 for log reduction of concentration, converts Eq. 15 to the following

$$\eta_{\mathrm{HCE}} = \frac{k_{\mathrm{m}} x_{\mathrm{c}} d_{\mathrm{c}} (1-\varepsilon_{\mathrm{b}}) \mathrm{PF}}{f v_{\mathrm{o}}} = \frac{Sh a_{\mathrm{c}} x_{\mathrm{c}} d_{\mathrm{c}} (1-\varepsilon_{\mathrm{b}}) \mathrm{PF}}{f Re Sc} \qquad (15)$$

Figure 9 illustrates the theoretical comparison of heterogeneous contacting efficiency (η_{HCE}) vs. inlet velocities for monoliths and MFECs. The η_{HCE} values were calculated based on Eq. 15. For theoretical comparison, the performance order was similar to the experimental comparison. The choice of these correlations used in this study was based on the operating conditions, bed properties, *Re*, and *Sc*. A different correlation might slightly change the values but would not significantly alter the η_{HCE} value trends obtained in this study.

Kinetic modeling

Figures 10 and 11 show the comparisons between the model predicted conversions and the experimental conversions for flat-shaped and W-shaped MFECs, respectively, based on the kinetic study discussed in Reaction Kinetic Modeling for Pleated MFEC Section. The conversion predicted by the kinetic model considered both surface reaction rate and mass-transfer rate as the experimental conversion result had shown that the operation was not solely in the mass-transfer controlled regime. The model predictions were in reasonable agreement with the experimental values for flat structures. For W-shaped structure, the experimental values differed from the model predictions. This difference can be attributed to the actual velocity inside the media and the change in media thickness due to the media compressibility. As the nickel fibers are malleable in nature, the voidage of media decreases due to compression, which eventually reduces the media thickness. Voidage and media thickness play significant roles in conversion measurement, according to Eq. 11. Furthermore, due to the pleated formation, vortices might form at the entrance of the structure. As discussed before, during actual velocity (inside the MFEC) calculation by the inclusion of PF term, these vortices were not taken into account which might result slight difference in actual velocities. These explain the difference between the model-predicted conversions and the experimental conversions for the W-shaped MFEC.

Table 6. Comparison among W-Shaped MFEC and Flat-Shaped MFEC

Structures	Activation energy, E_a (kJ/mol)	Intralayer Residence time[a] (μs)	Reynolds Number,[a] Re
W-shaped MFEC	40.9 ± 5	2750–275	2.84–28.4
Flat MFEC	42.9 ± 3	690–69	11.4–114

[a]Values are calculated based on $T = 473$ K.

The VOC removal kinetics follows a first-order rate law.[21,22] The kinetic modeling was fitted by tuning the surface reaction rate for a particular temperature. An Arrhenius plot for different pleated MFEC is shown in Figure 12. Based on the conversion result at different temperatures, activation energies for pleated MFECs were calculated and are shown in Table 6. For all cases, the total amounts of Pd and Mn were kept constant. Although the MFECs were differently pleated, the activation energies were almost equal for both pleated configurations. Furthermore, Table 6 contains the information of intralayer residence times and *Re* numbers corresponding to the operating conditions. As mentioned before, pleating and small characteristic dimension of the MFECs enhanced the laminar behavior inside the media. The intralayer residence time corresponded to the space time in the reactor geometry. As the MFEC thickness and the effective velocities were substantially low due to pleating, these reduced the residence times inside the media.

In the above experiments, MFEC reactor operation was not in the interphase mass-transfer controlled regime, and hence, there is further scope for improving the reactant conversion in MFEC by increasing the catalytic activity. Hence, a higher catalytic activity and a higher temperature will affect more positively to the performance of MFEC. As the ethanol conversion was very low, the bed compositions and properties of the MFECs require further optimization. The bed properties and compositions of the MFECs can be easily tailored based on the specific application. Hence, our future work will be MFEC optimization and operate it in interphase mass-transfer controlled regime in order to achieve better conversion.

Conclusions

Head-to-head experimental contacting efficiency comparison (i.e., pressure drop and chemical conversion comparisons) of wash-coated monoliths and pleated MFECs were performed in this study for VOC removal. The results showed that W-shaped MFEC exhibited improved performance than 230 CPSI and 400 CPSI monoliths. This increase in performance was the result of decreased effective velocity (inside the MFEC) due to the pleated formation. The decreased effective velocity lowered the pressure drop and increased the intralayer residence time which resulted better conversion. However, monoliths performed better relative to the MFECs of low pleat numbers because of the low resistance to flow and better conversion. The theoretical performance comparison verified the experimental trend. Furthermore, a reaction kinetic model was developed for the pleated MFEC to predict the global reaction parameters for high mass throughput systems. The model considered an isothermal plug flow reactor model and Peffer's equation. The model has shown reasonable agreement with the

experimental findings. Using this kinetic model, it would be possible to design better and more practical pleated MFEC configuration.

Pleated MFEC showed promising performance as it provided a large surface/volume ratio for the entrapped catalyst. This attribute facilitates the weight and volume demand of the air handling system in a limited space. Furthermore, microstructured reactor system provides the designer with the opportunity to "engineer the microfibrous properties of the media" to the desired intraparticle or intraparticle transport rates required to feed the embedded kinetics of the applications. The efforts were made to provide "second generation" structured reactor as compared to the conventional packed bed reactor and wash-coated monolith. As this study showed some remarkable advantages of pleated MFEC, further improvements of MFEC bed properties and compositions (Pleat numbers, voidage, catalyst loading, etc.) appear to be very promising.

Acknowledgments

The authors acknowledge the financial support by U.S. Army Tank-Automotive Research, Development and Engineering Center (TARDEC) under the contract no. W56HZV-05-C-0686 and the technical assistance of Mr. Troy Barron and Ronald Putt on the control and duct system. The authors would also like to thank Sasol Limited for their generous supply of products.

Notation

a_i = external surface area per unit volume of solid component i, m^{-1}
a_p = external surface area per unit volume of particles, m^{-1}
a_c = external catalyst surface area per unit volume of catalyst, m^{-1}
C_A = gas-phase concentration of reactant, ppm
C_{Ai} = inlet concentration of reactant, ppm
C_{Ao} = outlet concentration of reactant, ppm
C_D = coefficient of drag ($C_D=\frac{30}{Re_p}+\frac{67.289}{e^{5.03\varphi}}$)
C_f = coefficient of friction
C_{FD} = coefficient of form drag, ($C_{FD}=C_D-C_f$)
Cr = correction factor
D_m = molecular diffusivity, m^2/s
D_e = effective diffusivity inside catalyst
d_c = characteristic length of reactor, m
d_i = diameter of the solid component i, m
d_{ch} = monolith channel width, m
d_p = catalyst particle diameter, m
E_A = activation energy of reaction, kJ/mol
f = friction factor
f_F = Fanning friction factor
Gz = Graetz number, $Re_{ch}Scd_{ch}/L$
k_{eff} = effective reaction rate per unit catalyst volume, s^{-1}
k_f = gas-phase mass-transfer coefficient, m/s
k_m = $k_f a_c$, s^{-1}
k_r = surface reaction rate per unit catalyst volume, s^{-1}
L = length/thickness of reactor bed, m
M_i = molecular weight of gas component i, g/mol
M_{AB} = $2[(1/M_A)+(1/M_B)]^{-1}$, g/mol
ΔP = pressure drop across the reactor, kPa
Pe = reactor Peclet number
PF = pleat factor
Re = Reynolds number, $d_c v_o \rho/\mu$
Re_{ch} = Reynolds number based on monolith channel width, $d_{ch} v_o \rho/\mu$
Re_p = Reynolds number based on particle diameter, $\varphi_p d_p v_o \rho/\mu$
Sc = Schmidt number, $\mu/\rho D_M$
Sh = Sherwood number
T = temperature, K
t_w = catalyst wash-coat thickness, m
t_c = monolith wall thickness, m
x = position along the reactor length, m
x_{FD} = form drag parameter, $\varepsilon_b^2/12(1-\varepsilon_b)$
x_i = volume fraction of solid component i
x_c = volume fraction of catalyst support particles
W = function of γ, $W=2-3\gamma+3\gamma^5-2\gamma^6$

Greek letters

ρ = gas density, kg/m^3
ρ_c = catalyst support density, kg/m^3
μ = gas viscosity, kg/m s
τ_b = bed tortuosity, $1+(1-\varepsilon_b)/2$
τ_p = particle tortuosity
γ = $(1-\varepsilon_b)^{1/3}$
ε_b = bed void fraction
ε_p = intraparticle voidage
θ = flow path angle through bed
φ_i = sphericity of solid component i
φ_p = sphericity of particles
v_o = superficial gas velocity, m/s
η = internal effectiveness factor
Φ = Thiele modulus
η_{HCE} = heterogeneous contacting efficiency

Literature Cited

1. Liu W, Wang Y, Wilcox W, Li S. A compact and high throughput reactor of monolithic-structured catalyst bed for conversion of syngas to liquid fuels. *AIChE J*. 2012;58:2820–2829.
2. Liu W. Ministructured catalyst bed for gas-liquid-solid multiphase catalytic reaction. *AIChE J*. 2002;48:1519–1532.
3. Ouyang X, Bednarova L, Besser RS, Ho P. Preferential oxidation (PrOx) in a thin-film catalytic microreactor: advantages and limitations. *AIChE J*. 2005;51:1758–1772.
4. Cao C, Hu J, Li S, Wilcox W, Wang Y. Intensified Fischer-Tropsch synthesis process with microchannel catalytic reactors. *Catal Today*. 2009;140:149–156.
5. Tatarchuk B, Rose M, Krishnagopalan A, Zabasajja J, Kohler D. Mixed fiber composite structures high surface area high conductivity mixtures. US Patent 5,304,330. April 19, 1994.
6. Tatarchuk B, Rose M, Krishnagopalan A, Zabasajja J, Kohler D. Preparation of mixed fiber composite structures.US Patent 5,080,963. January 14, 1992.
7. Tatarchuk B, Rose M, Krishnagopalan A, Zabasajja J, Kohler D. Mixed fiber composite structures.US Patent 5,096,663. March 17, 1992.
8. Chang BK, Lu Y, Yang HY, Tatarchuk BJ. Facile regeneration vitreous microfibrous entrapped supported ZnO sorbent with high contacting efficiency for bulk H_2S removal from reformate streams in fuel cell applications. *J Mater Eng Perform*. 2006;15:439–441.
9. Lu Y, Sathitsuksanoh N, Yang HY, Chang BK, Queen AP, Tatarchuk BJ. Microfibrous entrapped ZnO-support sorbents for high contacting efficiency H_2S removal from reformate streams in PEMFC applications. In: Wang Y, Holladay JD, editors. *Microreactor Technol Process Intensification*, Vol. 914. 2005:406–422.
10. Yang H, Lu Y, Tatarchuk BJ. Glass fiber entrapped sorbent for reformates desulfurization for logistic PEM fuel cell power systems. *J Power Sources*. 2007;174:302–311.
11. Yang HY, Cahela DR, Tatarchuk BJ. A study of kinetic effects due to using microfibrous entrapped zinc oxide sorbents for hydrogen sulfide removal. *Chem Eng Sci*. 2008;63:2707–2716.
12. Kalluri RR, Cahela DR, Tatarchuk BJ. Microfibrous entrapped small particle adsorbents for high efficiency heterogeneous contacting. *Sep Purif Technol*. 2008;62:304–316.
13. Kalluri RR, Cahela DR, Tatarchuk BJ. Comparative heterogeneous contacting efficiency in fixed bed reactors: opportunities for new microstructured systems. *Appl Catal B*. 2009;90:507–515.
14. Wahid S, Tatarchuk BJ. Catalytic material with enhanced contacting efficiency for VOC removal at ultra-short contact time. *Ind Eng Chem Res*. 2013;52:15494–15503.
15. Nagda NL, Rector HE. A critical review of reported air concentrations of organic compounds in aircraft cabins. *Indoor Air*. 2003;13:202–301.
16. Balakotaiah V, West DH. Effective models for packed-bed catalytic reactors. *Chem Eng Sci*. 1999;54:1621–1638.
17. Giani L, Groppi G, Enrico T. Mass-transfer characterization of metallic foams as supports for structured catalysts. *Ind Eng Chem Res*. 2005;44:4993–5002.
18. Peffer R. Heat and mass transport in multiparticulate systems. *I&EC Fundam*. 1964;3:380–383.

19. Fogler H. *Elements of Chemical Reaction Engineering*, 4th ed. New Jersey: Prentice-Hall, Inc., 2006.
20. Kalluri RR. *Microfibrous Entrapped Catalysts and Sorbents: Microstructured Heterogeneous Contacting Systems with Enhanced Efficiency*. Auburn, AL: Auburn University, 2008.
21. Nimlos MR, Wolfrum EJ, Brewer ML, Fennell JA, Bintner G. Gas-phase heterogeneous photocatalytic oxidation of ethanol: pathways and kinetic modeling. *Environ Sci Technol*. 1996;30:3102–3110.
22. Kuo KK. *Principles of Combustion*, 2nd ed. Wiley, 2005.
23. Fuller EN, Schettler PD, Giddings JC. A new method for prediction of binary gas-phase diffusion coeffecients. *Ind Eng Chem*. 1966;58:19–27.
24. Plana C, Armenise S, Monzon A, Garcia-Bordeje E. Process optimisation of in situ H_2 generation from ammonia using Ni on alumina coated cordierite monoliths. *Top Catal*. 2011;54:914–921.
25. Garcia-Bordeje E, Kvande I, Chen D, Ronning M. Carbon nanofibers uniformly grown on gamma-alumina washcoated cordierite monoliths. *Adv Mater*. 2006;18:1589–1592.
26. Garcia-Bordeje E, Kvande I, Chen D, Ronning M. Synthesis of composite materials of carbon nanofibres and ceramic monoliths with uniform and tuneable nanofibre layer thickness. *Carbon*. 2007;45:1828–1838.
27. Nijhuis TA, Beers AE, Vergunst T, Hoek I, Kapteijn F, Moulijn JA. Preparation of monolithic catalysts. *Catal Rev Sci Eng*. 2001;43:345–380.
28. Tronconi E, Beretta A. The role of inter- and intra-phase mass transfer in the SCR-DeNO(x) reaction over catalysts of different shapes. *Catal Today*. 1999;52:249–258.
29. Heck RM, Farrauto RJ. *Catalytic Air Pollution Control: Commercial Technology*. New York: Van Nostrand Reinhold, 1995.
30. West DH, Balakotaiah V, Jovanovic Z. Experimental and theoretical investigation of the mass transfer controlled regime in catalytic monoliths. *Catal Today*. 2003;88:3–16.

Manuscript received Mar. 26, 2014, and revision received June 22, 2014.